In press, Brain Topography, Jan. 2013

Effect of forward model errors on EEG source localization

Zeynep Akalin Acar, Scott Makeig

Swartz Center for Computational Neuroscience, Institute for Neural Computation, University of California San Diego 0559, La Jolla CA 92093-0559

Abstract

Subject-specific four-layer boundary element method (BEM) electrical forward head models for four participants, generated from magnetic resonance (MR) head images using NFT (sccn.ucsd.edu/wiki/NFT), were used to simulate electroencephalographic (EEG) scalp potentials at 256 recorded electrode positions produced by single current dipoles of a 3-D grid in brain space. Locations of these dipoles were then estimated using gradient descent within five template head models fit to the electrode positions. These were: a spherical model, three-layer and four-layer boundary element method (BEM) head models based on the Montreal Neurological Institute (MNI) template head image, and these BEM models warped to the recorded electrode positions. Smallest localization errors (4.1 mm to 6.2 mm, medians) were obtained using the electrode-position warped four-layer BEM models, with largest localization errors ($\approx$ 20 mm) for most basal brain locations. When we increased the brain-to-skull conductivity ratio assumed in the template model scalp projections from the simulated value (25:1) to a higher value (80:1) used in earlier studies, the estimated dipole locations moved outwards (12.4 mm, median). We also investigated the effects of errors in co-registering the electrode positions, of reducing electrode counts, and of adding a fifth, isotropic white matter layer to one individual head model. Results show that when individual subject MR head images are not available to construct subject-specific head models, accurate EEG source localization should employ a four- or five-layer BEM template head model incorporating an accurate skull conductivity estimate and warped to 64 or more accurately 3-D measured and co-registered electrode positions.

Key words:
EEG, Head Modeling, Boundary Element Method, BEM, spherical head model, MNI head model, white matter, skull conductivity, co-registration, electrode number.

1. INTRODUCTION

Localization of brain EEG sources is important for both clinical (Plummer 2008) and in basic brain research (Makeig 2004). Quantitative localization of EEG brain sources began in the 1950's with investigations of the nature of scalp surface potential distributions projecting from brain sources (Brazier 1949; Shaw 1955), and with solutions of the inverse source localization problem for single equivalent dipole sources within a best-fitting spherical head model (Henderson 1975; Schneider 1974). Subsequent research has continued to improve tools for accurate source localization. The three most important components of a successful source localization approach are, (a) an electric forward head model for the subject, (b) a ('source space') model of possible source locations, and (c) an inverse source localization method. Here, we use simulations based on realistic individual subject forward head models to investigate source localization errors produced by inaccuracies introduced by use of template head models (not based on a subject MR head image), inaccurate skull conductivity estimates, imprecise electrode co-registration, and low electrode numbers.

Neuronal electric activity that can be measured outside the scalp by EEG (and its magnetic counterpart, MEG) originates primarily from groups of neurons organized in macrocolumns perpendicular to the cortex surface (Baillet 2001). A physiologically relevant assumption is to construct the source space using 'patches' of the cortical surface, based on the observation that metabolically active areas are closely related to active neuron groups (Lutkenhoner 1995;

☆This work is supported by NIH (2R01NS047293), and a gift from The Swartz Foundation.
Email addresses: zeynep@sccn.ucsd.edu (Zeynep Akalin Acar), scott@sccn.ucsd.edu (Scott Makeig)

Baillet 1997). A useful approach is to use equivalent current dipoles to model coherent electrical activity arising in small cortical areas (de Munck 1988). Although it has been shown that extended sources may be localized deeper in the brain using a single dipole approximation (Lucka 2012), equivalent dipole models are efficient for modeling smaller cortical EEG or MEG sources. We showed by simulation studies that synchronous field activity across a compact patch of cortex has a projection to the scalp nearly equaling that of an equivalent dipole source located near the center of the patch (Akalin Acar 2012). Maximum localization error introduced by modeling the patch source as a current dipole was 2 mm for patches 10 mm in radius. Since it is possible to obtain highly 'dipolar' scalp maps of active EEG brain sources (e.g., scalp maps highly resembling the projection of a single equivalent dipole) by decomposing high-dimensional EEG data using Independent Component Analysis (ICA) (Delorme 2012), here we used single dipoles to simulate equivalent brain sources.

The most important source of localization error in solutions to the EEG inverse problem is the forward head model employed. Studies investigating dipole source localization accuracy using spherical or spheroidal head models have reported mean errors of 10 mm to 30 mm (Cohen 1990; Henderson 1975; Weinberg 1986; Zhang 1993; Zhang 1994). These simple geometric models allow computationally efficient analytic solutions but lack proper representation of head shape and thus typically produce relatively poor results. Subject-specific head models built from magnetic resonance (MR) head images using the Boundary Element Method (BEM) (Akalin Acar 2004), Finite Element Method (FEM) (Gencer 2004; Wolters 2002), or Finite Difference Method (FDM) (Vanrumste 2000) volume conduction models allow more accurate calculation of scalp electrical (or magnetic) fields arising from cortical sources. Typically, subject-specific head models are constructed by segmentation and mesh generation of an individual subject MR head image.

Studies comparing source localization using spherical head models and three-layer realistic BEM models observed a reduction in model-based error by 10-20 mm for simulated EEG (Buchner 1995; Crouzeix 1999; Cuffin 1996; Kobayashi 2003; Roth 1993; Vatta 2010) and by 2.5-12 mm for simulated MEG source dipoles (Crouzeix 1999; Yvert 1997). Roth et al. (Roth 1993) reported a 20-mm improvement in average source localization accuracy in frontal and temporal lobes, with improvements of more than 40 mm in some cases. In another study, Buchner et al. (Buchner 1995) performed a similar analysis for dipolar sources in the central sulcus region and reported an up to 7-mm improvement, mainly attributed to inadequate modeling of local head geometry by the spherical model. They pointed out that mis-localization was more prominent for deeper source locations estimated using a spherical head model. Yvert et al. (Yvert 1997) and Crouzeix et al. (Crouzeix 1999) reported localization differences induced by a spherical head model ranging from 2.5 mm in superior to 12 mm in inferior brain areas. The degree of complexity of the head model also affects the accuracy of forward and inverse problem solutions. Ramon et al. (Ramon 2006) used FEM models to examine the effects of soft skull bone, cerebrospinal fluid (CSF) and gray matter on scalp potential distributions. Wendel et al. (2008) analyzed the effect of CSF on EEG sensitivity. These studies concluded that a multi-layer model including the CSF layer is required to obtain accurate inverse source localization estimates.

Another important consideration determining the accuracy of both forward and inverse problem solutions is correct modeling of head tissue conductivities, especially the conductivity ratio of the skull relative to brain and scalp. Experimental studies have reported consistent conductivity values for scalp, brain, and CSF tissues. However, huge variations in skull conductivity may arise from differences in measurement methods (Oostendorp 2000) as well as from normal variations in skull conductivity from person to person and through developmental changes throughout the life cycle (Hoekema 2003).

A few researchers have reported measurements of isolated skull conductivity values (while part of the skull was temporarily removed for clinical purposes) (Hoekema 2003; Oostendorp 2000), while other conductivity estimates have been obtained from EEG, MEG, or ECoG measurements (Baysal 2004; Gutierrez 2004; Lai 2005; Lew 2009). Other methods used to estimate skull conductivity include current injection, magnetic field induction, and MR-based electrical impedance tomography (MREIT) (Ferree 2000; Gao 2005; Ulker Karbeyaz 2003). Reported brain-to-skull conductivity ratios have varied between 10:1 and 80:1. Van Uitert et al. (2004) studied how tissue conductivity estimation errors influence the MEG inverse problem. They found up to 6.2-mm localization differences when assumed skull conductivity was changed by only 10% from its simulated ground-truth value. Dannhauer et al. (2011) have also shown effects on EEG source localization of local conductivity variations over the skull surface.

Another source of errors in solutions to EEG inverse problems is improper co-registration of the electrode positions, typically recorded using a 3-D digitizer, especially if head fiducial points are not digitized. Automatic co-registration of these relative locations to the head model may depend on the accuracy of an initial visual co-registration (Akalin Acar 2010). Khosla et al. (1999) investigated electrode mislocalizations of about 5 degrees using spherical head models and reported mean 8-mm localization errors.

The aim of this study was to use simulated source location and EEG scalp potential data to systematically explore the effects of forward modeling errors on solutions to simulated EEG inverse problems, and to present a more thorough analysis of forward modeling errors on EEG source localization. To do this, we generated several different head models for four adult participants: first realistic, subject-specific models constructed from subject MR head images, and then best-fitting spherical and four types of template-derived head models. EEG head modeling errors were examined assuming an individual MR head image was not available but the digitized electrode locations were available.

Next, for a rectangular 3-D grid of dipole locations inside the brain volume in the realistic head model of each of the four subjects, we computed simulated EEG scalp potential maps of projections to an array of 256 scalp electrode positions and then estimated the dipole source locations using the spherical and four template-based head models for each subject. This provided a 3-D estimate of source localization error introduced by inaccuracies in template-based forward head models used in inverse dipole source localization. We used the same methods to investigate the effects of white matter modeling, inaccuracy in electrode co-registration, reduction in sensor number, and errors in skull conductivity estimation. When examining the effects of skull conductivity mis-estimation, electrode co-registration errors, and addition of a WM layer to realistic head modeling, we assumed both the individual MR and the digitizer locations were available. Our aim was to better understand and document how different types of forward modeling errors affect the localization of EEG sources in different parts of the brain.

2. Head models

Measured T1-weighted MR head images and 256-channel electrode montage positions from four adult subjects (2 female, 2 male) were used to construct or adapt electrical head models. MR images were acquired using a 3-T GE scanner with 1-mm voxel resolution. Two of the subjects were European American, one was Turkish, and one was Korean. For each subject, six head models were constructed:

1. *Subject-specific (realistic) reference head model (RLS-4)*: A four-layer, $\approx 20,000$-node BEM model representing brain, CSF, skull, and scalp was generated from the T1-weighted whole-head MR image of each subject. To investigate how different types of forward modeling errors contribute to mis-estimation of source locations in different parts of the brain, we constructed the forward reference model sources without introducing additional measurement noise (which should also be present in actual EEG inverse problems).
2. *Four-layer MNI head model (MNI-4)*: A four-layer, 16,497-node template BEM model was generated from the Montreal Neurological Institute (MNI Colin27) template head model (`www.bic.mni.mcgill.ca/ServicesAtlases/Colin27`).
3. *Three-layer MNI head model (MNI-3)*: A three-layer, 12,498-node template BEM model representing brain, skull and scalp was generated from the MNI template head model.
4. *Warped four-layer MNI head model (wMNI-4)*: The four-layer template BEM model was warped to the measured subject electrode positions.
5. *Warped three-layer MNI head model (wMNI-3)*: A three-layer template BEM model warped to the 3-D electrode position measured from the subject.
6. *Spherical head model (SPH)*: A three-layer concentric spherical model was fit to the measured subject electrode positions. The radii of the inner layers were in proportion to the values given by Meijs et al. (Meijs 1989) (65, 71 and 75 mm for brain, skull and scalp respectively).

The subject-specific reference head models were used to generate simulated EEG scalp potentials from the simulated current dipole sources. For all models, brain and scalp conductivities were assigned the value 0.33 S/m (Geddes 1967). The value 1.79 S/m was used for CSF conductivity. This value has been shown to be reliable across subjects (Baumann 1997). The brain-to-skull conductivity ratio used in the models was 25:1 (Lai 2005). The locations of equivalent dipoles were then estimated using each of the other five models.

We used the NFT toolbox (`sccn.ucsd.edu/wiki/NFT`) (Akalin Acar 2010) to generate the head models as illustrated in Figure 1. NFT allows users to generate realistic three- or four-layer head models from a T1-weighted 3-D MR head image. It can also build three- or four-layer template-based head models by warping the template MNI model to the recorded electrode positions. This allows users to obtain a head model closer to the subject's true head shape when the subject's MR image is not available. Warping procedure starts with an initial co-registration using three fiducial points: the nasion and left and right preauricular points. After this initial co-registration, 19 landmarks are located on both the head model and sensors. The landmarks on the MNI model are pre-calculated and saved. They

are loaded with the MNI head mesh when warping starts. The corresponding landmarks on the sensors are calculated automatically. These landmarks are used to find the best-fitting warping parameters using a non-rigid thin plate spline method (Darvas 2006; Bookstein 1999). All the surfaces and the source space are warped using the same warping parameters. This results in more realistic head models compared to mapping electrodes to a template mesh. Reverse warping parameters that warp the sensor coordinates to the template mesh are also computed. These parameters can be used to map source localization results to the original template head model (Akalin Acar 2010). Co-registration of electrode locations with fixed MNI models also starts with an initial co-registration and locating landmarks, then a rigid transformation is applied, and finally the electrode locations are projected on the MNI scalp surface.

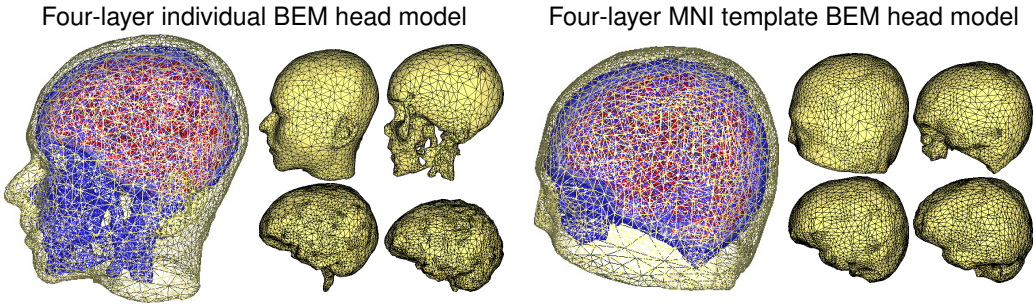

Figure 1: A realistic head model generated from a subject T1-weighted whole head MR image (left) and an MNI template model fit to the same (subject S1) head (right). The four shells of the BEM models (scalp, skull, CSF, and grey matter) are shown to the right of each model.

Here we asked whether warping the model head shape to the measured electrode positions (wMNI) was more accurate than warping the measured electrode positions to the fixed template head model (MNI). Results of the head model warping for the four subjects with co-registered electrode locations are shown in Figure 2. After warping, median sensor distance from the template model scalp mesh decreased by 3-7 mm. Figure 3 shows scalp, skull, CSF and brain tissue boundaries for a four-layer MR-based realistic, a four-layer warped MNI, and a four-layer MNI head models plotted on a sagittal slice of subject S1.

3. EEG head modeling errors

EEG head modeling errors were examined assuming an individual MR head image is not available but the digitized electrode locations are available. To assess localization errors for dipole sources located anywhere in the brain, the EEG scalp potential maps were simulated in the subject-specific reference head models (RLS-4) for a rectangular 3-D grid of dipole locations with 8-mm spacing through the cortical volume. To better understand the effect of source orientation on source localization, three orthogonal (x, y, z oriented) simulated dipoles were placed at each grid location. (Here x ran anterior to posterior, y left to right, and z bottom to top of the head). The resulting 3-D grid source spaces for the four subjects comprised 6,075-7,512 dipoles (at 2,025-2,504 grid locations). For each subject, the simulated scalp projections of each dipole source to the 256 scalp electrodes were then localized in the five template head models, using gradient descent seeded by the best-fitting location in the subject source-space grid. Note that simulations were performed without adding sensor (or other) noise. Therefore the localization errors presented in this section represent a best-case scenario with ideal signal-to-noise ratio (SNR).

In BEM modeling, as the dipoles get closer to a surface, numerical inaccuracy increases. Here, we set the minimum distance of a dipole to the brain surface to 2 mm. In previous studies we compared our BEM implementation accuracy using spherical head models (Akalin Acar 2010; Akalin Acar 2004). Using a four layer spherical model with 61-, 65-, 71-, and 75-mm radii (Meijs 1989), all with 1,026 nodes per layer, we obtained a 1.7% change in scalp map topographies even when the dipoles were located 1 mm away from the brain surface.

3.1. Error graphics for one subject

We first present results for one subject (S1). Figure 4 shows the equivalent dipole source localization error directions and magnitudes for the spherical (top row) and the four MNI-template based head models for this subject, computed from source dipole scalp projections simulated using the reference MR image-based four-layer forward head model. Localization errors for three sets of equivalent source dipoles oriented in the x, y, and z directions, respectively,

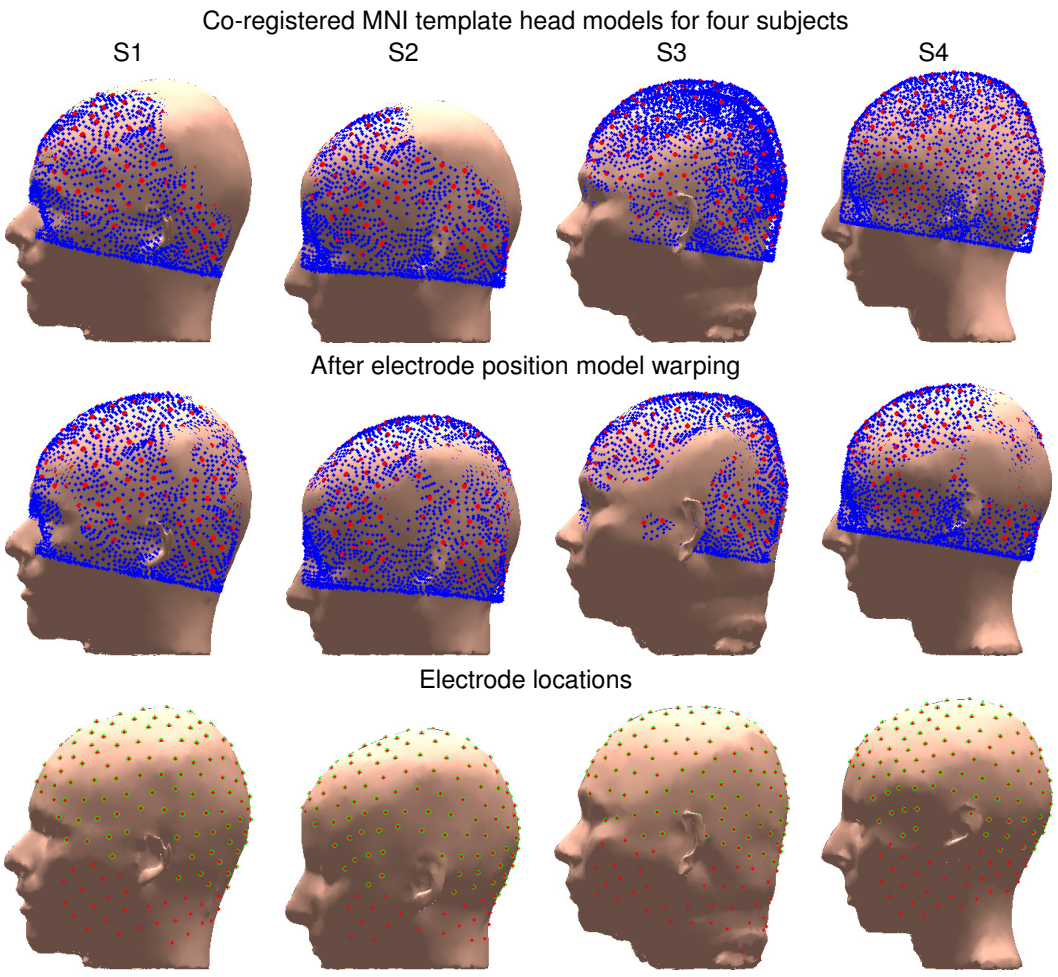

Figure 2: Registered (upper row) and head shape-warped (middle row) MNI template model scalp meshes plotted on the scalp surface of the reference head models with co-registered MNI electrode locations. Co-registered electrode locations with the subjects' scalp surfaces (red dots) and selected electrodes used in MNI and spherical head model source localization (green circles) are shown in the lower row.

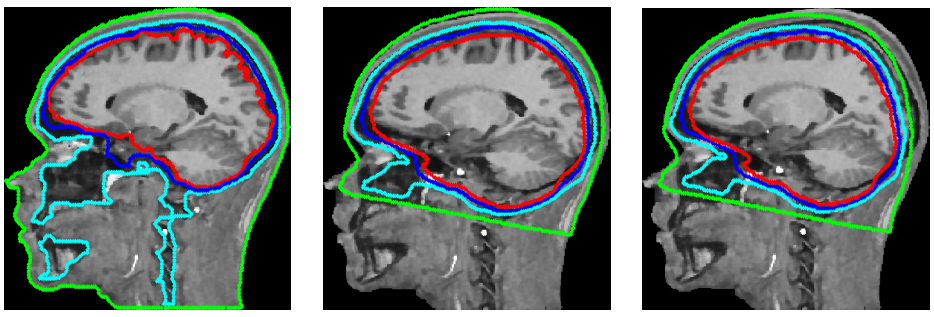

Figure 3: Scalp, skull, CSF and brain tissue boundaries for (a) four-layer MR-based realistic, (b) four-layer warped MNI, and (c) four-layer MNI head models plotted on a sagittal slice of subject S1.

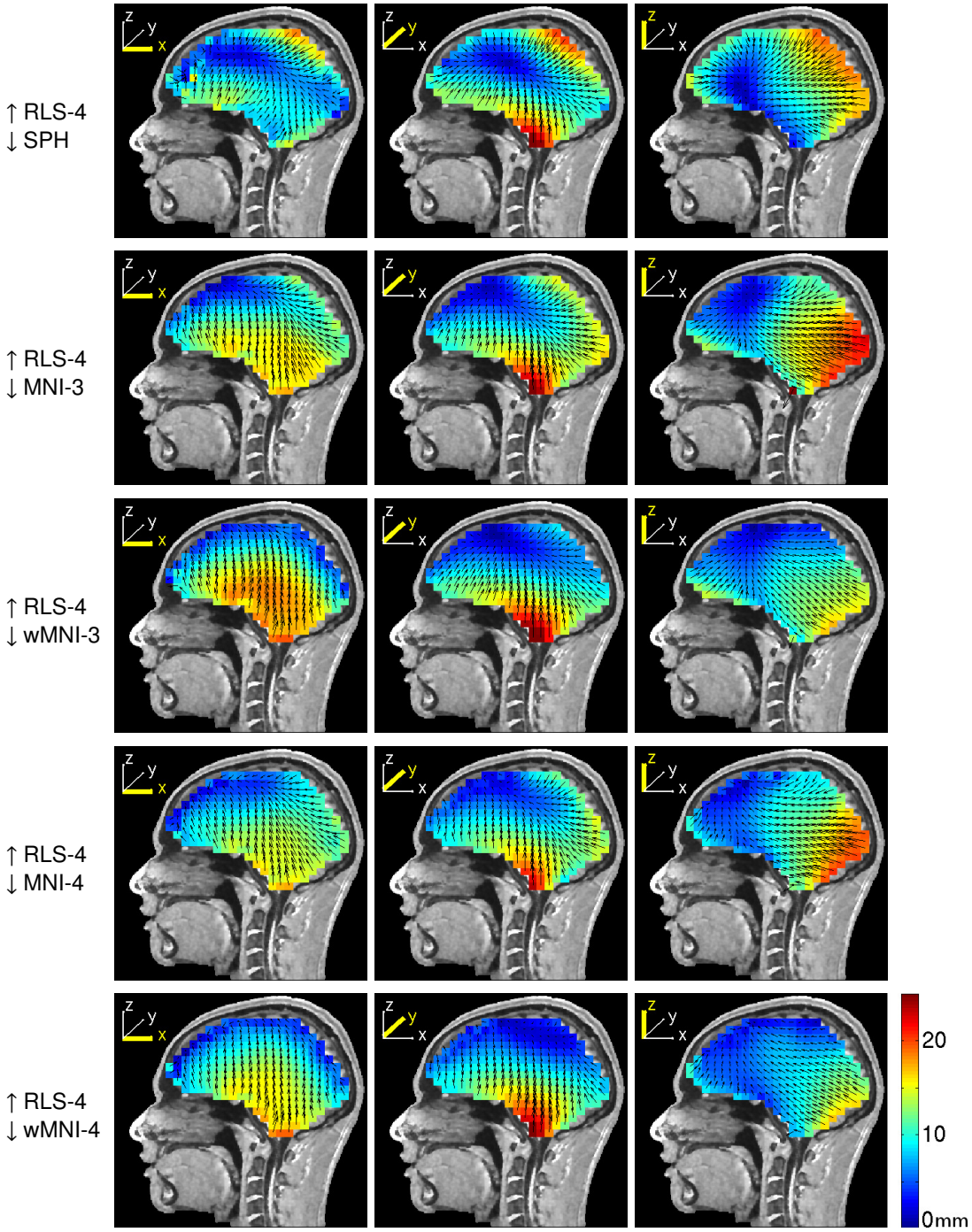

Figure 4: Equivalent dipole source localization error directions (arrows) and magnitudes (colors) for spherical (top row) and four MNI-template based head models computed from source dipole scalp projections computed using a four-layer realistic subject MR image based BEM forward head model (subject S1 in Figure 2). The forward and inverse models are indicated to the left of each row (↑: forward model, ↓: inverse model). The source space was a regular Cartesian grid of single current dipole sources with 8-mm spacing filling the brain volume. The three columns show the errors for equivalent dipole sources that were oriented in x-, y-, and z-directions, respectively (see insets). Note that, maximum error shown was 25 mm so as to use the same scaling for all the plots while retaining some contrast for the lower-error plots. Maximum localization errors were given in Table 3.

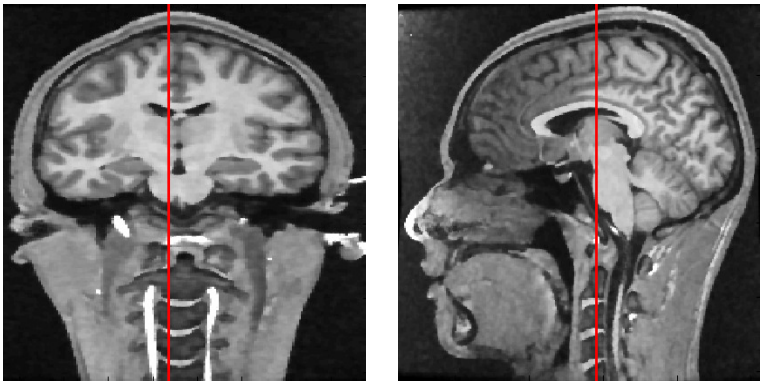

Figure 5: Selected coronal and sagittal slices to show localization errors.

were computed for 7,512 dipoles through the whole brain volume. Localization errors are shown for dipoles in one sagittal slice at $y = 87$ *mm* (4 mm from the central sulcus) (Figure 5).

In general, dipole localization errors were smaller than 30 mm for both the spherical head model and for the MNI models. Localization errors were largest in inferior brain where the spherical models diverged the most from the reference head models. The MNI-template head models captured overall head shape better. However, since the template MNI head does not model the whole head (below the nose), the MNI-template head models did not model current flow accurately in the base of the brain. Some of the inferior electrode positions located below the lower limit of the MNI-template model had to be omitted. This factor further increased localization errors for source dipoles located in the inferior portion of the MNI head models.

In the three-layer MNI head models, the CSF was combined with the cortical layer. Four-layer MNI-template head models (wMNI-4, MNI-4) improved source localization over three-layer models (wMNI-3, MNI-3) by up to 8 mm. Improvement was especially prominent here in frontal cortex. Localization differences of up to 10 mm were observed between the head model warped and electrode position-warped (MNI) models. Because of differences in head shape, details of these differences varied across subjects.

To assess localization errors for dipole sources with varying orientations, we simulated EEG scalp potential maps for dipoles with 18 regularly distributed directions on a sphere using the realistic BEM head model for subject S1. To avoid increasing the number of dipoles tested by a factor of 6, we increased the grid spacing to 16 mm and decreased the number of dipole locations to 314. We selected the 18 dipole orientations by dividing each face of an octahedron into 4. As the errors were the same for opposite dipole directions, the effective total number of dipole orientations was 9. We used the four-layer subject-specific realistic BEM model as the reference model, and a four-layer warped MNI model to reconstruct the sources. Localization errors were slightly smaller for some radially oriented dipoles than for dipoles oriented in the 3 Cartesian directions (especially x-directed dipoles).

To obtain a more quantitative analysis, we found the dipole direction with maximum localization error for each grid location. While at 114 of the 314 voxels, x-directed dipoles were localized with largest localization error, this was true for radial dipoles at fewer than 23 voxels. Table 1 gives the number of voxels with maximum localization error for each direction. Also Figure 6 shows maximal direction errors for voxels in a sagittal and a coronal slice of the brain.

3.2. Results across four subjects

The analysis described in the previous section was repeated for three more subjects with different head shapes (Figure 2). Figure 7 shows magnitude-sorted localization error distributions for the four subjects (S1-4). In general, four-layer head-shape warped MNI-template head models gave source location estimates closest to the simulated source locations in the MR-based reference head models. For some subjects (S2 and S4) spherical models produced the largest localization errors, however for other subjects (S1 and S3) the localization errors obtained by using a spherical model were comparable to the MNI template models. For the four-layer warped MNI models, half of the dipole location estimates had errors smaller than 4.1-7.8 mm (depending on subject).

Figure 8 shows, for each of the four subjects (S1-4), the histogram of percent residual variance (PRV) over the dipoles in the source space. The PRV measures the residual field in the scalp projections of the simulated dipoles not accounted for by the projections of the source estimates. The histogram is normalized to show the percentage of the

px	py	pz	Median error (mm)	Number of voxels
1	0	0	9.1	114
0	1	0	7.6	20
0	0	1	7.0	58
-0.7071	0.7071	0	8.2	45
-0.7071	-0.7071	0	8.2	25
-0.5	0.5	0.7071	7.8	23
-0.5	-0.5	0.7071	7.9	14
0.5	-0.5	0.7071	6.0	7
0.5	0.5	0.7071	5.9	8

Table 1: Median error and number of dipole locations with maximum localization errors for 9 different dipole orientations. Columns px, py, and pz represent dipole coordinates in x, y , and z directions.

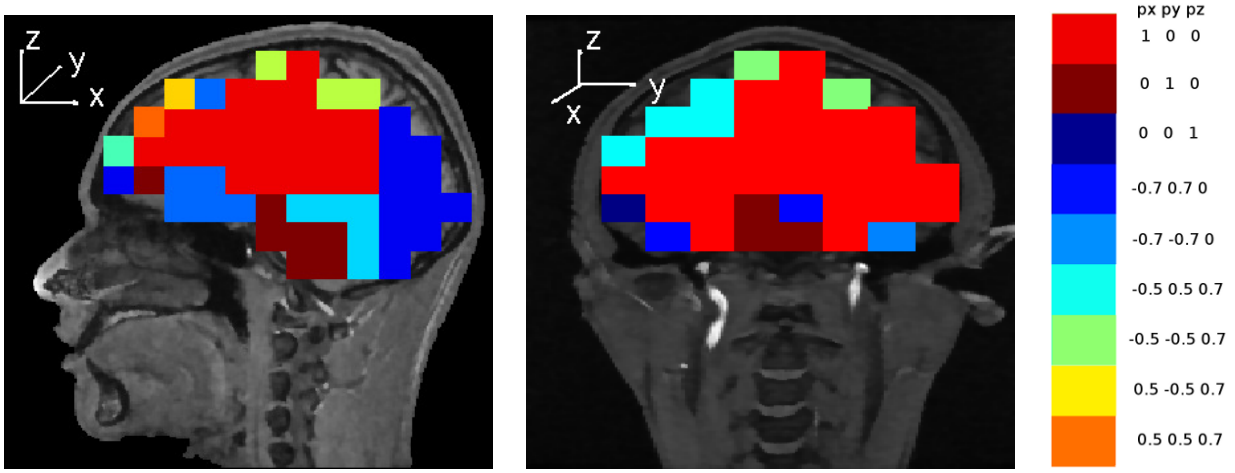

Figure 6: Sagittal and coronal slice dipole-error maps showing, for each slice-transversed voxel, the dipole direction with the largest localization error.

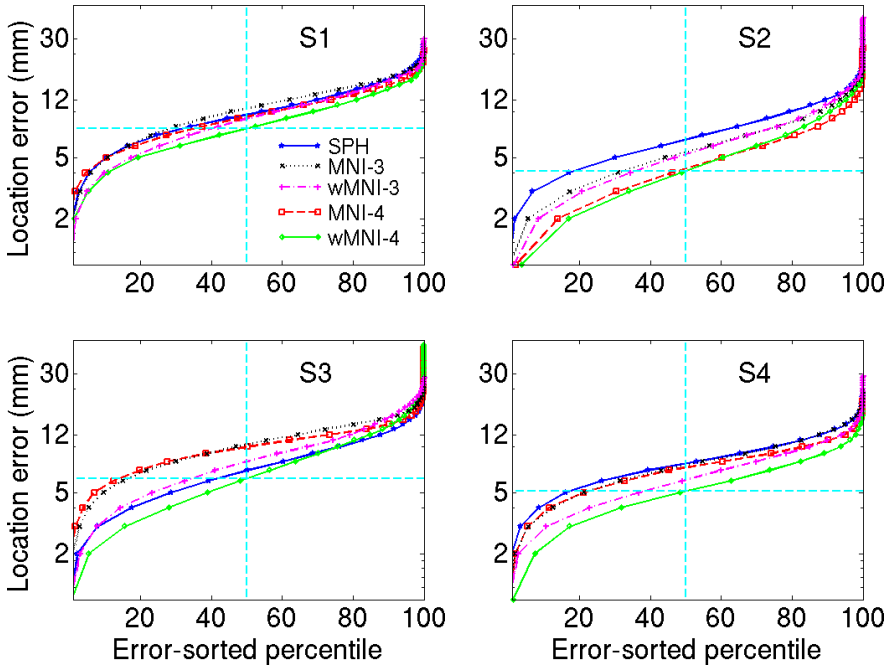

Figure 7: Magnitude-sorted localization error distributions in four subjects (S1-4) for source localization performed using spherical (blue) or MNI template-based head models, each showing best localization prformance for the 4-layer electrode position-warped MNI template head model (wMNI-4).

	SPH	**MNI-3**	**wMNI-3**	**MNI-4**	**wMNI-4**
S1	9.5	10.5	9.0	9.3	7.8
S2	6.6	5.5	5.3	4.3	4.1
S3	7.0	10.3	8.0	10.0	6.2
S4	7.8	7.6	6.1	7.3	5.1
Mean	8.4	7.6	6.5	7.0	5.4

Table 2: Median dipole source localization error magnitudes (in mm) for four subjects (plus the mean model) when the inverse problem is solved using spherical and MNI head models adapted to the subject head shape.

dipoles that has the corresponding PRV. Although, all of the head model estimates gave similarly low (1%) residual variances, the warped four-layer MNI models (green) produced the least PRV.

Next, we co-registered the other three subjects MR images to the MR image of subject S1 using Freesurfer volume registration (`surfer.nmr.mgh.harvard.edu`). Localization error magnitude and orientation maps were interpolated to a 1-mm 3-D grid of source locations from the 8-mm spaced source location grids. These error maps were then transformed to the S1 coordinate system to obtain mean error maps across the four subjects using the same volume registration for the source space. As the subject head shapes were quite different, in some brain regions the co-registered error directions differed, thus partly cancelling each other in the mean error images. Figure 9 shows the mean dipole source localization error directions (arrows) and magnitudes (colors), and Table 2 the median localization error magnitudes (in mm).

4. Effect of white matter modeling

Next, we explored the effects of adding a fifth white matter (WM) layer to one of the reference head models (S1). Several studies have investigated the effects of the anisotropy of white matter conductivity (Gullmar 2010; Hallez 2008; Ramon 2006; Wolters 2006). Here, we show equivalent dipole source localization results for sources through the brain volume, but using BEM models that cannot take into account tissue anisotropy.

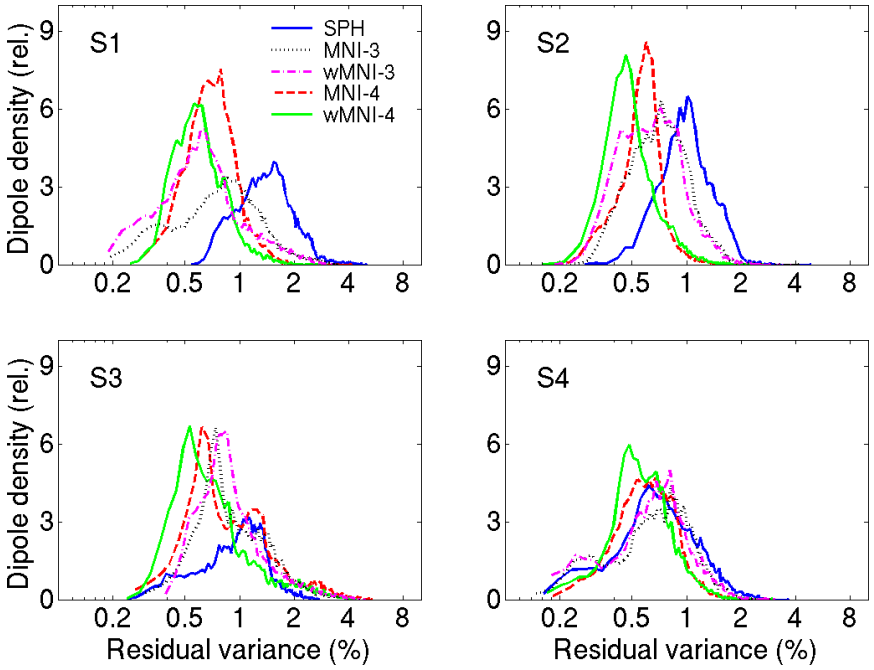

Figure 8: Histograms of percent residual scalp map variance for source estimates based on spherical or MNI-based head models for the four subjects (S1-4), each showing best fits for the 4-layer electrode position-warped MNI template head model (wMNI-4) and poorest fits for the spherical model (SPH).

To add a white matter layer in our BEM model, we used the Freesurfer white matter segmentation (Figure 10, left). We then generated a white-matter mesh using a FreeSurfer tool by decimating the surface to 10,240 faces (Figure 10, right). Here, we used 0.14 S/m as isotropic white matter conductivity (Gullmar 2010). EEG current dipole source scalp potential maps were then simulated in this five-layer reference head model. Finally, dipole source localization was performed using the four-layer reference model and the four-layer warped MNI head model for this subject.

Source localization errors produced by the four-layer reference model, ignoring the white matter layer, were largest for z-directed dipoles located just below the WM (median error, 2.8 mm; maximum, 18.6 mm). Localization changes for dipole sources above (or within) the WM region were relatively low (Figure 11, top row). The four-layer head-shape warped MNI model (Figure 11, bottom row), gave localization error distributions similar to those obtained using the four-layer reference model (Figure 4, bottom row).

5. Co-registration errors

When it is not feasible to use MR-visible capsules during MR imaging to allow skin landmark-based co-registration of the measured EEG electrode positions to the MR-derived head model, co-registration of electrode positions may depend on an initial visual co-registration. Electrode position measurement in NFT (Akalin Acar 2010) consists of two steps. First, a manual co-registration is accomplished using the subject's head model scalp mesh and digitized electrode positions. This is followed by an automatic co-registration step to find 6 translation and rotation parameters that minimize the total squared distance between the sensors and the model scalp surface. This process is valid whether fiducial locations are digitized or not. While use of fiducials minimizes co-registration errors, some laboratories do not measure fiducial locations. In these cases the co-registration may depend on an initial visual co-registration. Here, we may expect some tilt in the co-registered electrode positions, especially backwards or forward. Thus, we calculated equivalent dipole source localization error directions and magnitudes for one four-layer reference BEM head model (S1) when the co-registered electrode montage was mistakenly tilted 5 degrees backwards or 5 degrees to the left (Figure 12). Even though random electrode displacements have been reported to not have much effect on EEG source localization (Wang 2001), here when we shifted the simulated electrode positions in one direction we observed up to 12-mm localization errors that were largest for superficial dipoles closest to the electrode positions.

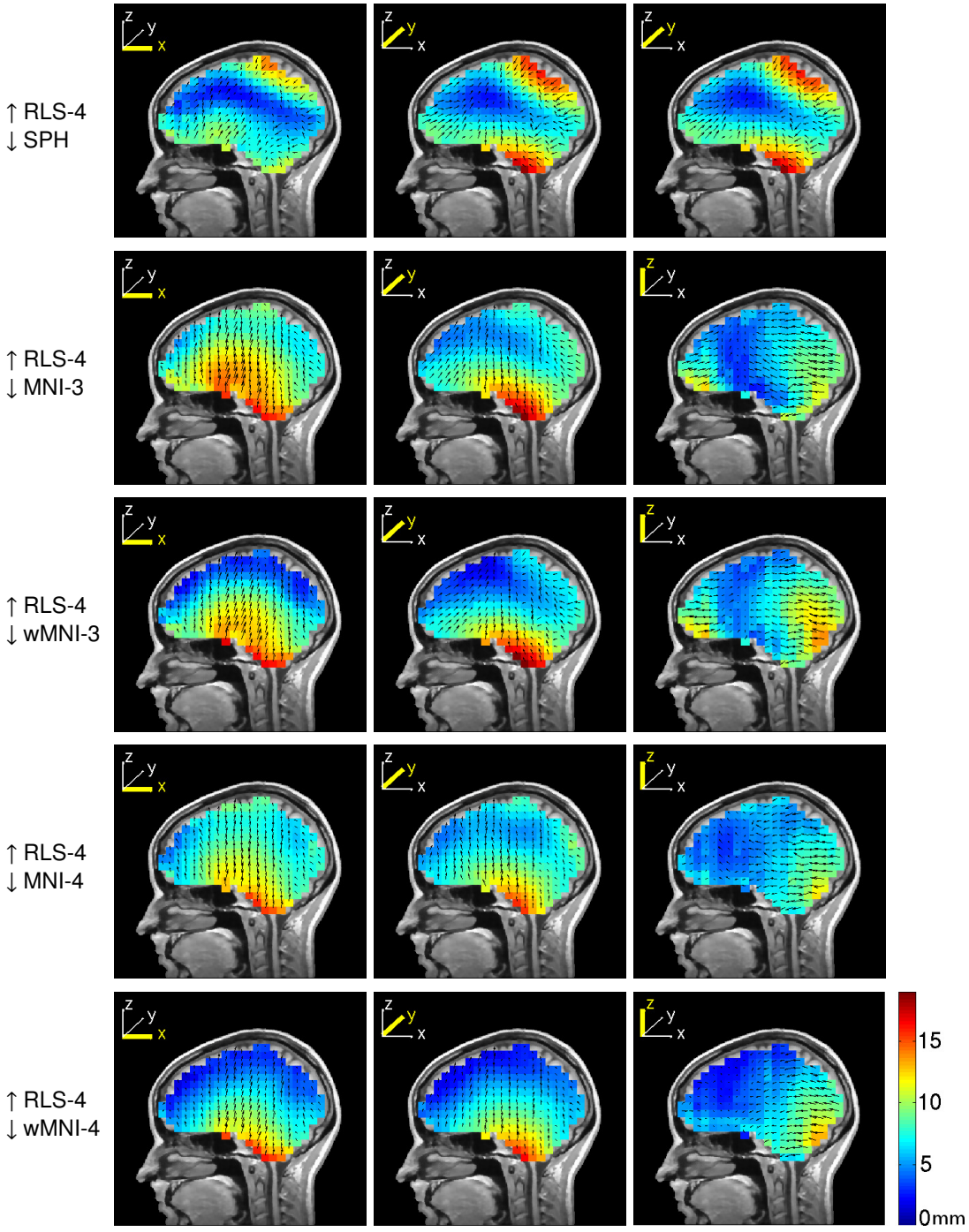

Figure 9: Mean dipole source localization error directions (arrows) and magnitudes (colors) for four subjects using spherical and MNI template-based head models to localize equivalent dipole sources simulated in a subject-specific four-layer realistic BEM head model. Other details as in Figure 3.

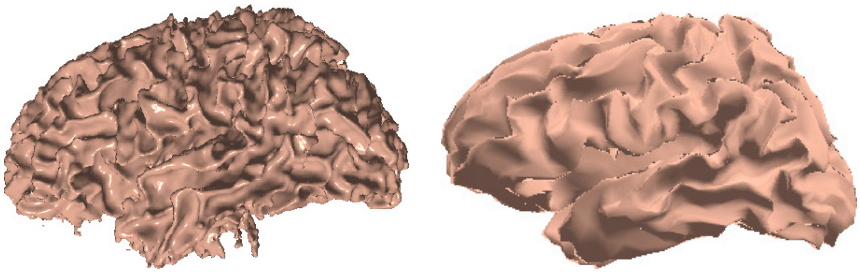

Figure 10: High-resolution white matter segmentation obtained using Freesurfer (left), and the decimated BEM white matter mesh (right) consisting of 10,240 triangular faces.

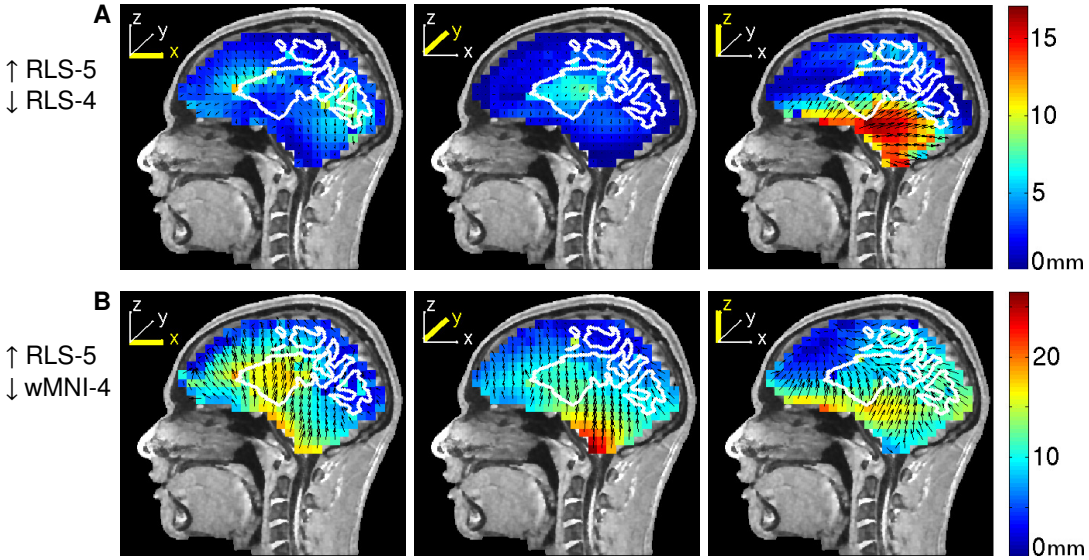

Figure 11: Equivalent dipole source localization error directions (arrows) and magnitudes (colors) relative to simulated dipole projections using a four-layer reference head model (S1) for EEG data simulated using a five-layer BEM head model including a white matter layer. The white matter boundary in the five-layer model is outlined in white. Other details as in Figure 3.

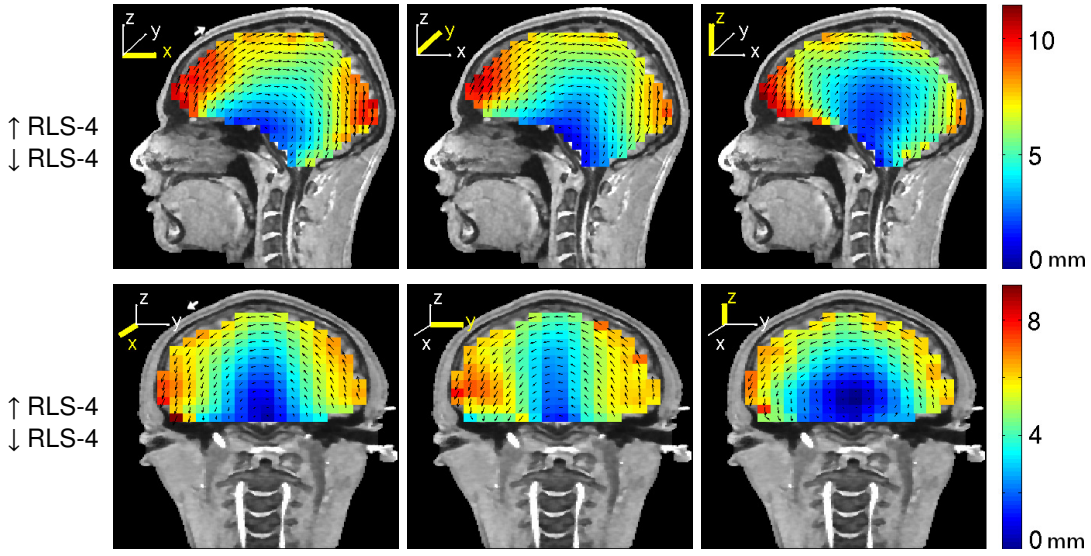

Figure 12: Equivalent dipole source localization error directions (arrows) and magnitudes (colors) in a four-layer reference BEM head model when the co-registered scalp electrode positions were tilted 5 degrees backwards (top row), or 5 degrees to the left (bottom row) before dipole localization. White arrows in the leftmost panels show the approximate size of the simulated location error. Other details as in Figure 3.

6. Conductivity estimation errors

Next, we present simulation results on the effects of using incorrect skull conductivity values on equivalent dipole source localization. In the 1970's and 80's, the adult brain-to-skull conductivity ratio was reported to be near 80:1 (Cohen 1983; Rush 1968), a value still commonly used for EEG source localization. However, more recent studies have found this ratio to be lower, as low as 15:1 (Oostendorp 2000). For example, a 2005 study on adult epilepsy patients undergoing pre-surgical evaluation using simultaneous intra-cranial and scalp EEG recordings estimated average brain-to-skull conductivity ratio as 25:1 (Lai 2005).

Here, we used the four-layer reference BEM model for subject S1 and set the forward-model (ground truth) brain-to-skull conductivity ratio to 25:1. We then solved the inverse source localization problem using the same head model incorporating the assumed (and still commonly used) value of 80:1. This produced large equivalent dipole localization errors of up to 31 mm (Figure 13, top row). When we used the four-layer head-shape warped MNI template model to solve the inverse problem (Figure 13, middle row) the errors were still larger and more evenly distributed across the cortical region (Figure 4 bottom row). The estimated positions of the simulated dipoles generally moved towards the scalp surface. Conversely, when the brain-to-skull conductivity ratio was mis-estimated as 15:1 instead of 25:1 (Figure 13, bottom row), the estimated dipole locations moved towards the center of the brain, with error magnitudes up to 13 mm. Thus, correct modeling of skull conductivity is an important factor for EEG source localization, quite possibly outweighing the choice of head model.

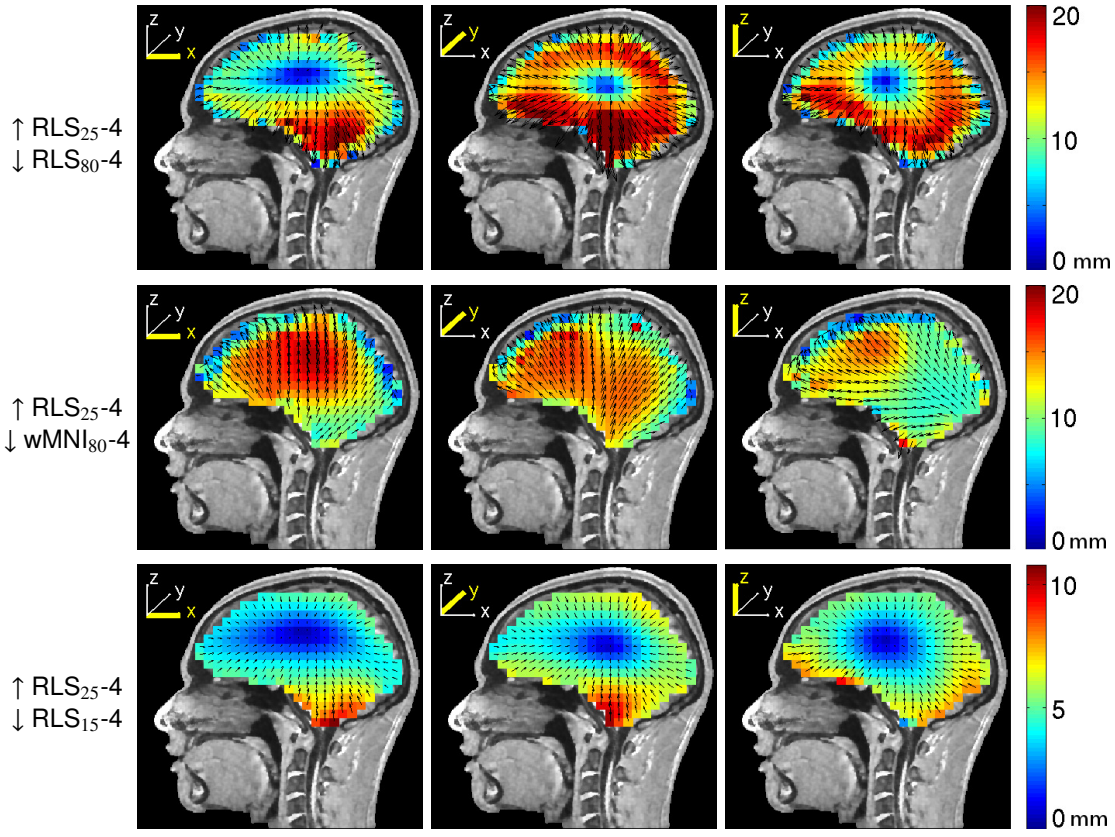

Figure 13: Equivalent dipole source localization error directions (arrows) and magnitudes (colors) for model dipoles in a four-layer realistic BEM head model when the brain-to-skull conductivity ratio was mis-estimated as 80:1 (top row) or as 15:1 (bottom row) instead of the simulated forward-model value (25:1). The middle row shows errors when source localization was performed using a warped four-layer MNI head model and the forward model brain-to-skull ratio was again mis-estimated as 80:1. Note that, maximum error shown was 20 mm for top and bottom rows so as to use the same scaling while retaining some contrast for the lower-error plots. Maximum localization errors were given in Table 3. Other details as in Figure 3.

7. Electrode number based errors

Another factor affecting the accuracy of EEG source localization is the number of recorded scalp sensors. When using the same model for forward and inverse problem solutions in (noise-free) simulations, varying the number and positioning of the electrodes did not produce appreciable changes in source location estimates. Here, we simulated the EEG scalp projections using the four-layer reference head model for subject S1 with 256 electrodes (Biosemi, Amsterdam). Using the same model would be 'cheating' ('inverse crime' (Kaipio 2007)), so we performed equivalent dipole estimation using the (next-best) four-layer head-shape warped MNI model but with smaller numbers of electrodes (192, 128, 64, 32, and 16) with positions fairly evenly distributed over the scalp surface.

Sometimes, scalp electrodes cannot be placed uniformly on the scalp surface (Gunduz 2011). Thus, we also tested localization using 32 and 16 electrodes covering only the right hemisphere. Figure 14 shows the 256 electrode positions on the reference model scalp surface, the electrode montages for the wMNI models with smaller numbers of electrodes, and 32- and 16-electrode montages over the right hemisphere only (R32 and R16). Figure 15 shows the error magnitude and direction estimates for a four-layer head-shape warped MNI head model using 192 electrodes (from Figure 4) and the additional errors introduced by using only 16 uniformly distributed electrodes or using 16 electrodes covering only right side of the head. Figure 16 shows magnitude-sorted localization error distributions. Localization errors did not change for 192 or 128 electrodes, but larger source localization errors occurred when the number of electrodes was 64 or less. The maximum and average changes in localization error were 6.3 and 0.6 mm when 64 electrodes were used instead of 192 electrodes, 7.8 and 1.3 mm when 32 electrodes were used, and 8.4 and 2.7 mm when only 16 electrodes were used. Note that, in Figure 15, maximum error shown was 25 mm so as to use the same scaling for all the plots while retaining some contrast for the lower-error plots. Maximum localization errors were 62 mm for the R16, and 32 mm for the 16 electrode montages (Table 3). These results are consistent with those reported in (Michel 2004; Mosher 1993).

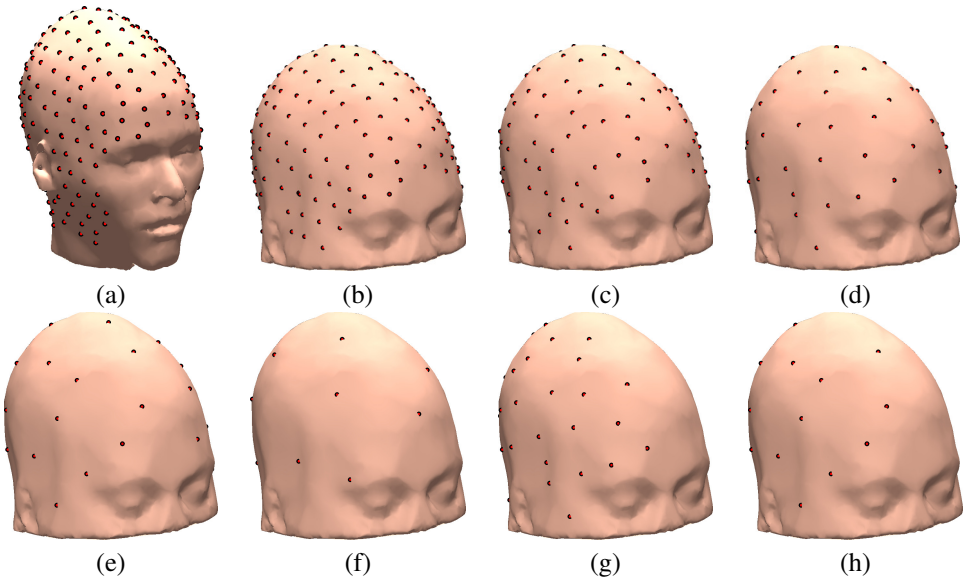

Figure 14: (a) 256 sensor locations on the S1 reference head model, (b-f) 192, 128, 64, 32, and 16 distributed sensor locations on the S1 head shape-warped (wMNI-4) template model, (g-h) 32 and 16 sensor locations placed only on the right side of the template model.

The scalp coverage of the electrode montage plays an important role as well. We obtained larger localization errors using 32 electrodes placed only on the right side of the head than using only 16 more uniformly distributed electrodes. When the electrodes were placed only on the right side of the head, the localization errors were largest for dipoles in the left side of the brain.

8. Comparison of forward modeling errors

To give an overall quantitative understanding of forward modeling errors, we segmented several cortical regions (Figure 17) using Freesurfer and present average and maximum equivalent dipole localization errors for different

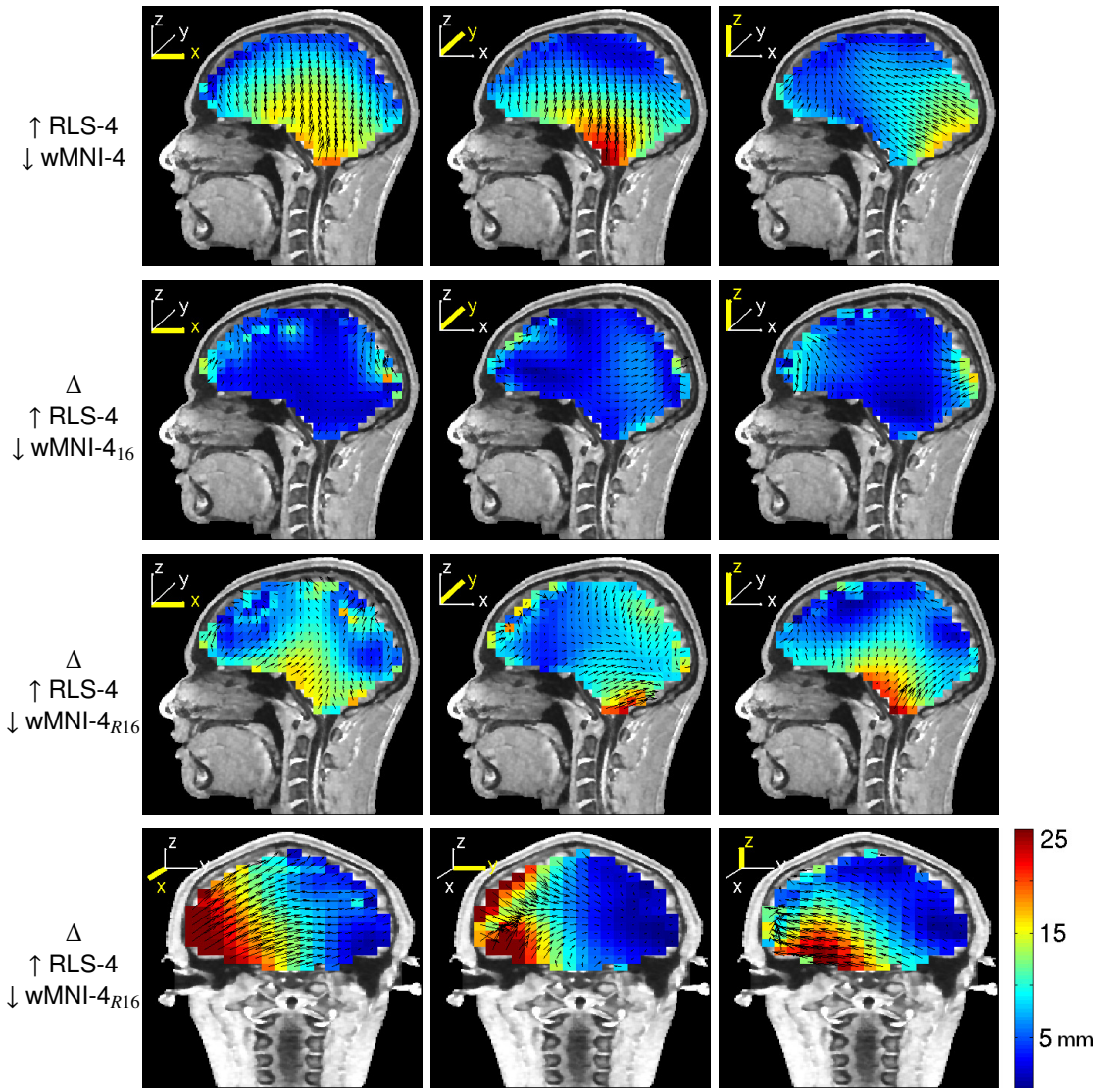

Figure 15: Top-row: Equivalent dipole source localization error directions (arrows) and magnitudes (colors) for a head shape-warped four-layer MNI head model using 192 electrodes (from Figure 3). The lower three rows show additional errors introduced by using only 16 uniformly distributed electrodes (subscript 16, second row), or using 16 electrodes covering only right side of the head (subscript R16, bottom rows).

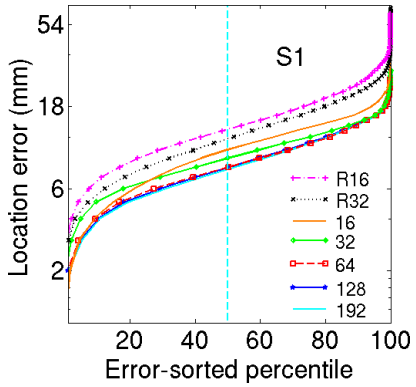

Figure 16: Magnitude-sorted localization error distributions (subject S1) for source localizations performed using the sensor distributions shown in Figure 14 (c-h) and the wMNI-4 template head model.

forward models in Table 3. Sub-cortical and cerebellar voxels are also grouped into one class. Modeling errors were higher in areas where head model geometry differed most from the actual geometry of the head. The localization errors observed when the assumed skull conductivity ratio was highly inaccurate (80:1 instead of 25:1) were comparable to the relatively large modeling errors arising from use of a spherical model. Sub-cortical and cerebellar regions were less affected by sensor registration errors. Smallest template model errors were obtained using a four-layer warped MNI model with 64 or more near-uniformly distributed sensors. It should be remembered, however, that all our estimates here assume that the source being estimated has a valid single equivalent-dipole model (e.g., represents the projection to the scalp of local field activity wholly or partially synchronous across a single cortical patch), and that the scalp map representing its projection has been captured with ideal SNR.

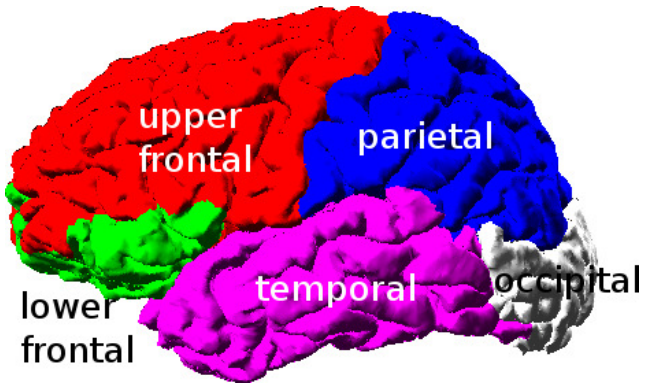

Figure 17: Cortical regions of subject S1 brain. Segmentation obtained using FreeSurfer.

9. Computational Complexity

Table 4 shows the computation times and memory size of the forward model matrices for a realistic BEM head model with 20,000 vertices, run on a 3.2-GHz 64-bit Intel Xeon CPU. We used the Isolated Problem Approach, which requires computation of three BEM matrices (Akalin Acar 2010; Akalin Acar 2004). While the BEM matrix generation is resource intensive it is possible to reduce the computation times by parallelization (Ataseven 2008).

10. Discussion and Conclusion

Here, we investigated effects of several common forward modeling errors on EEG source localization using simulation studies. We simulated errors in head model geometry, skull conductivity estimation, electrode co-registration, white-matter modeling, and insufficient channel density. EEG scalp potential maps were simulated for a regular 3-D grid of 6,075-7,512 current dipoles located throughout the brain volume projecting in three orthogonal directions. Simulated EEG scalp maps were generated using subject-specific four- or five-layer BEM reference models generated from subject MR head images. To examine head modeling errors, source localization was performed using spherical and four types of MNI template-based head models. Since the model errors depend in part on the subject's head geometry, we repeated these simulations for four different subjects with relatively different head geometries. The simulations are free of sensor noise and influence of other brain or non-brain EEG activity. Therefore, they represent an ideal case; in practice, sensor noise and interference from other source activities may be expected to increase localization errors, particularly for deeper dipoles.

MNI Template head model errors: Though localization accuracy using different head models varied across subjects, four-layer actual head-shape warped MNI models produced dipole locations closest to their locations in the reference head models, with median localization errors of about 5 mm. Since the MNI head template does not extend below the brain itself, inverse models based on this template are still not optimal. The truncation of the head model below the brain resulted in increased localization errors for sources located near the bottom of the head model. The results are in agreement with previous research indicating that such errors would be smaller if the head model were extended below the brain (Bruno 2003; Lanfer 2012). Better results may be obtained using a template model that represents the whole head (Valdes-Hernandez 2009). We conclude that when collection of MR head images for each

		Head model			Conductivity ratio (assumed)		Co-registration		# of sensors	Coverage	
Cortical Areas		SPH	warped MNI 4-layer	5-layer model (with w. m.)	80:1	15:1	5-deg back	5-deg left	16 (balanced)	16 (imbalanced) right	left
Upper Frontal	Mean	7.7	5.1	2.2	10.6	4.4	6.6	4.9	7.1	8.5	15.9
	Max	20.9	14.0	13.4	19.1	7.4	12.0	8.3	20.4	16.4	37.8
Lower frontal	Mean	10.2	8.0	3.1	12.1	5.1	6.3	3.7	8.8	10.8	15.8
	Max	24.2	15.0	13.5	28.5	9.4	12.2	7.4	17.6	21.7	50.4
Temporal	Mean	12.3	9.4	4.1	12.8	5.6	2.8	5.0	11.7	7.4	12.8
	Max	27.9	20.0	16.2	29.9	12.5	7.1	9.4	23.1	23.7	62.4
parietal	Mean	10.3	10.1	3.6	12.9	5.4	6.2	2.6	13.2	11.6	18.0
	Max	20.3	15.0	11.7	19.4	8.0	9.1	8.3	26.6	18.2	33.8
occipital	Mean	10.6	6.1	2.5	11.4	4.5	5.2	4.4	8.6	11.1	24.2
	Max	18.7	16.9	15.0	21.7	8.2	11.7	6.4	32.0	17.8	23.7
Sub-cort. cerebellum	Mean	10.2	11.2	4.2	13.5	5.1	3.9	3.3	12.2	14.4	20.5
	Max	27.0	27.0	18.6	31.8	13.0	8.9	7.1	29.3	36.1	54.9
Total	Mean	10.2	8.4	3.4	12.2	5.0	4.9	4.1	10.3	10.8	18.2
	Max	27.9	27.0	18.6	31.8	13.0	12.2	9.4	32.0	36.1	62.4

1

Table 3: Average and maximum source localization errors for different sources of forward modeling errors in different brain regions.

	Computational complexity	Memory
Generation of BEM matrices	107 min	4.5 GB + 1.9 GB + 1.1 GB
Calculation of the transfer matrix	9.3 min	124.1 MB
Calculation of the lead field matrix	47 min	14.4 MB

Table 4: Computational complexity for a realistic model with 20,000 vertices.

EEG subject is not possible, using some other method to estimate subject head shape is desirable – e.g., 3-D electrode position measurement, for which a more reliable method may be to use photogrammetric methods (Russell 2005) for which solutions based on sequential photographs of the (stationary) subject head are now becoming more widely available (see, for example, `123dapp.com/catch`).

Spherical head model errors: Localization errors obtained using spherical head models were comparable with localization errors obtained with MNI models in two subjects and were larger for the other two subjects. In general, the distribution of the errors was also similar with the MNI head models, however the errors were larger in the occipital region. We used the same electrodes as in the MNI models (Figure 2, bottom row - green circles) co-registered to the spherical models. When we used all the electrodes in the realistic models (including those positions in Figure 2 shown using red dots), since the cheek and neck electrode positions were not near their positions in the best-fitting spherical head models we obtained higher localization errors (up to 40 mm, 12.4-mm mean). Thus, when spherical head models are used for source localization, any cheek and neck electrodes should be omitted for better source localization. We also performed simulations using four-layer spherical head models for all four subjects and compared the error magnitudes and distributions with those obtained by using three-layer spherical head models. Localization errors obtained using three- and four-layer spherical head models were very similar – the average localization error differed by only 1-2 mms, and the error distributions were the same.

White-matter layer: We also examined the effects of introducing a fifth white matter layer into the reference BEM models and observed a movement of up to 18.6 mm for vertically-oriented basal dipoles located beneath the superior cortex white matter region. Change in estimated dipole locations for superior dipole locations was relatively small (median change, 3.4 mm).

Electrode co-registration error: To examine the effects of electrode co-registration errors on EEG source localization, we shifted the electrode positions by 5 degrees in one direction, as might occur during visual co-registration of the set of relative electrode positions obtained using a 3-D digitizer. This shifted each electrode position by 6-7 mm and produced source localization errors of up to 12 mm for superficial sources, with median localization errors of 4-5 mm.

Skull conductivity error: Mis-estimation of skull conductivity is an important source of error in forward problem solutions. To test the effects of incorrect skull conductivity, we solved the inverse problem using assumed brain-to-skull conductivity ratios (80:1 and 15:1) differing from the simulated 'ground-truth' value (25:1) used in the forward projections. Using inaccurate estimates of skull conductivity produced large localization errors, for 80:1 up to 31 mm for dipoles close to the skull with a median 12-mm localization error; and still appreciable (13-mm, maximum; 5-mm, median) localization errors for 15:1. When instead we solved the inverse problem with a four-layer electrode-positions warped MNI template model, the errors were more evenly distributed across the cortical region. The source estimates were closer to the skull surface when the too-high (80:1) brain-to-skull ratio (i.e., a too-low skull conductivity value) was assumed, while using a ratio (15:1) lower than the simulated ground-truth value produced deeper source estimates. These observations are aligned with the view that conductivity boundaries act as layers of secondary sources (Gencer 2004). EEG scalp maps sum the projections of the source dipole as well as its secondary sources at the brain-skull interface. When the inverse problem is solved assuming too low a skull conductivity, the located source moves towards the skull to compensate for the reduced magnitude of the secondary sources.

Current limitations: The RLS-4 and RLS-5 head models used as the reference models in this study include a detailed, subject-specific geometry of the whole head and include all major tissue types. However, there are still some limitations and approximations in these models:

Lack of anisotropy: Because we used BEM models, skull and white matter conductivities were simplified to use isotropic conductivity values. Effects on source localization of white matter anisotropy have been investigated in (Hauesien 2002; Wolters 2006; Gullmar 2010) and of skull anisotropy in (Marin 1998; Chauveau 2004). However, recent studies have shown that skull was originally assumed to be anisotropic because of its layered structure (Sadleir 2007; Dannhauer 1011). Instead of modeling the poorly conducting compacta and better conducting spon-

giosa layers separately using high-resolution meshes, the skull layer was approximated using large surface elements with anisotropic conductivity. A future study might compare effects of modeling skull inhomogeneity by modeling the compacta and spongiosa layers with an isotropic homogeneous and anisotropic homogeneous skull models. However, this approach would be computationally expensive, as when meshes are closer to each other higher-resolution meshes are required. An alternative approach to modeling thin skull layers and anisotropy is to use FEM models.

Simplifications in segmentation for BEM models: Our models used 4 or 5 tissue layers. A few studies have modeled as many as 11 or 12 different head tissues (Ramon 2006) even including blood vessels (Fiederer 2012). Here, sinuses were not modeled (Akalin Acar 2010). Traditional BEM implementations approximate tissue boundaries by closed surfaces and model the head using concentric, non-intersecting set of layers such as scalp, skull, CSF, brain and white matter. Though this approximation is not quite anatomically correct, it is widely used in BEM head modeling. The BEM implementation first described in (Akalin Acar 2004) is unique in the sense that it models tissue boundaries as surfaces that are created and combined in a way that allows modeling the eyes, any holes in the skull, and other large 'intersecting' tissue boundaries. Although our BEM formulation allows for intersecting tissue boundaries, an automatic mesh generation to create these intersecting tissues is not yet possible with NFT. Therefore, for simplicity, we created non-intersecting layers for tissue boundaries.

Effects of Noise: The simulations performed in this paper did not include noise. In the presence of noise, it may be expected that localization errors should increase, particularly for deep sources.

Single dipole search: While the single-dipole-search algorithm used in this work provides good results, it does not guarantee perfect convergence to the global minimum. Unfortunately, inverse algorithms that provide this guarantee were too expensive to use for the large number of source localizations performed for this paper.

In conclusion. Several factors affect the accuracy of EEG inverse problem solutions. When template models are used for source localization, errors are higher in brain regions in which the model most deviates from the subject's head geometry. Use of subject-specific MR-derived head models should therefore be preferred whenever possible. Of the template models we tested, a four-layer template head model warped to measured 3-D sensor locations on the subject scalp surface gave the best results. Our results also show that using correct conductivity values is at least as important as using the correct head geometry to solve the EEG inverse problem. For example, locating frontal lobe sources using a head-shape warped four-layer MNI template model introduced a mean 5.1-mm localization error, and tilting the co-registered electrode montage by five degrees produced an additional 6.6-mm mean error. However, conductivity mis-estimation (80:1 instead of 25:1) produced a mean 10.6-mm error. Estimating the head tissue conductivities during source localization is therefore an important area of research.

While using subject MR-image based finite element method (FEM) or finite difference method (FDM) head models incorporating diffusion-weighted imaging (DWI) based estimates of directional white matter anisotropy may produce still more accurate EEG source localization (Wolters 2002), individualized MR-based images are not available for many EEG studies. It may be possible to achieve a desirable (¡¡ 1cm) level of accuracy in many new and existing EEG-based functional cortical imaging studies by: 1) Using a model that accurately represents head geometry and electrode placement, 2) estimating skull conductance from the data (Huang 2007; Lew 2009), and 3) finding equivalent dipole source locations accounting for synchronous activity within relatively small, compact cortical patches (Akalin Acar 2009) - such as those derived by ICA decomposition of high-density data (Delorme 2012). In particular, this level of accuracy should allow useful comparison of data source locations across EEG and blood oxygenation level-dependent (BOLD) studies.

References

Akalin Acar Z, Gencer N.G. (2004): An Advanced BEM implementation for the forward problem of Electro-Magnetic Source Imaging. Physics in Med. and Biol 49(5):5011-5028

Akalin Acar Z, Makeig S. (2010): Neuroelectromagnetic forward head modeling toolbox. J. of Neuroscience Methods 190:258-270.

Akalin Acar Z., Makeig S. (2012): EEG cortical patch sources and equivalent dipole source localization. in preparation.

Akalin Acar Z, Worrell G, Makeig S (2009): Patch based electrcortical source imaging in epilepsy. IEEE Engineer Med Biol Soc 2009, Minneapolis, Minnesota, 2009.

Ataseven Y., Akalin Acar Z., Acar C.E., Gencer N.G. (2008): Parallel implementation of the accelerated BEM approach for EMSI of the human brain. Med. Biol. Eng. Comput. 46:671-679.

Baillet S, Garnero L. (1997): A Bayesian approach to introducing anatomo-functional priors in the EEG/MEG inverse problem. IEEE Trans. Biomed. Eng. 44(5):374-385.

Baillet S, Mosher J.C., Leahy R.M. (2001): Electromagnetic brain mapping. IEEE Signal Proc. Magazine 18(6):14-30.

Baumann SD, Wozny D.R., Kelly S.K., Meno. F.M. (1997): The electrical conductivity of human cerebrospinal fluid at body temperature. IEEE Trans. Biomed. Eng. 3:220-223.

Baysal U, Haueisen J. (2004): Use of a priori information in estimating tissue resistivities - application to human data in vivo. Physiological Meas. 25:737-748.

Bookstein F. 1999. Linear methods for nonlinear maps: procrustes fits, thin-plate splines, and the biometric analysis of shape variability. Brain warping. . New York: Academic Press. p 157-181.

Brazier MAB. (1949): A study of the electrical fields at the surface of the head. Electroenceph. clin. Neurophysiol. Suppl. 2:38-52.

Bruno P, Vatta F., Mininel S., Inchingolo P. (2003): Skull conductivity and extension of head volume conductor model: simulation of bioelectric phenomena. Proc of 25th annual int. conf. IEEE EMBS, Cancun, Mexico.

Buchner H, Waberski T.D., Fuchs M., Wischmann H.-A., Wagner M., Drenckhahn R. (1995): Comparison of realistically shaped boundary-element and spherical head models in source localization of early somatosensory evoked potentials. Brain Topography 2(8):137-143.

Chauveau N, Franceries X., Doyon B., Rigaud B., Morucci J.P., Celsis P. . (2004): Effects of skull thickness, anisotropy, and inhomogeneity on forward EEG/ERP computations using a spherical three-dimensional resistor mesh model. Human Brain Mapping 21(2):86-97.

Cohen D, Cuffin B.N. (1983): Demonstration of useful differences between magnetoencephalogram and electroencephalogram. Electroencep. and clin. neurophysiol. 56:38-51.

Cohen D, Cuffin N. B., Yunokuchi K., Maniewski R., Purcell C., Cosgrove R.G., Ives J., Keneddy J.G., Schomer L.D. (1990): MEG versus EEG localization test using implanted sources in the human brain. Annals of Neurology 28(6):811-817.

Crouzeix A, Yvert B., Bertrand O., Pernier J. (1999): An Evaluation of Dipole Reconstruction Accuracy with Spherical and Realistic Head Models in MEG. Clin. Neurophysiol. 110:2176-2188.

Cuffin NB. (1996): EEG Localization accuracy improvements using realistically shaped head models. IEEE Trans. Biomed. Eng. 44(3):299-303.

Dannhauer M, Lanfer B., Wolters C.H., Knosche T. R. (2011): Modeling of the human skull in EEG source analysis. Human Brain Mapping 32(9):1383-1399.

Darvas F, Ermer J., Mosher J., Leahy R. (2006): Generic head models for atlas-based EEG source analysis. Human Brain Mapping 27:129-143.

de Munck J, Van Dijk BW., Spekreijse H. (1988): Mathematical Dipoles are Adequate to Describe Realistic Generators of Human Brain Activity. IEEE Trans. Biomed. Eng. 35(11):960-966.

Delorme A, Palmer J., Oostenveld R., Makeig S. (2012): Independent EEG sources are dipolar. PLOS One.

Ferree T, Eriksen K., Tucker D. (2000): Regional head tissue conductivity estimation for improved EEG analysis. IEEE Trans. Biomed. Eng. 47:1584-1592.

Fiederer LDJ, et al. (2012): High-resolution forward modeling using finite element method head models based on 7T MRI data. HBM Proceedings 2012.

Gao N, Zhu S.A., He B. (2005): Estimation of electrical conductivity distribution within the human head from magnetic flux density measurement. Phys. in Med and Biol. 50:2675-2687.

Geddes LA, Baker L. E. (1967): The specific resistance of biological materials - A compendium of data for the biomedical engineer and physiologist. Med. Biol. Eng. 5:271-293.

Gencer NG, Acar C. E. (2004): Sensitivity of EEG and MEG measurements to tissue conductivity. Phys. Med. Biol. 49:701-717.

Gullmar D, Haueisen J., Reichenbach J.R. (2010): Influence of anisotropic electrical conductivity in white matter tissue on the EEG/MEG forward and inverse solution. A high-resolution whole head simulation study. Neuroimage 51:145-163.

Gunduz A, Brunner P., Daitch A., Leuthardt E.C., Ritaccio A., Pesaran B., Schalk G. (2011): Neural correlates of visual-spatial attention in electrocorticographic signals in humans. Frontiers in human neuroscience 5.

Gutierrez D, Nehorai A., Muravchik C. (2004): Estimating brain conductivities and dipole source signals with EEG arrays. IEEE Trans. on Biomed. Eng. 51:2113-2122.

Hallez H, Vanrumste B., Van Hese P., Delputte S., Lemahieu I. (2008): Dipole estimation errors due to differences in modeling anisotropic conductivities in realistic head models for EEG source analysis. Phys. Med. Biol. 53:1877-1894.

Haueisen J, Tuch D.S., Ramon C., Schimpf P.H., Wedeen V.J., George J.S., Belliveau J.W. (2002): The Influence of Brain Tissue Anisotropy on Human EEG and MEG. Neuroimage 15:159-66.

Henderson CJ, Butler S.R. (1975): The localization of equivalent dipoles of EEG sources by the application of electrical field theory. Neurophysiol. 39:117-130.

Hoekema R, Wieneke G.H., Leijten F.S.S., van Veelen C.W.M., van Rijen P.C., Huiskamp G.J.M., Ansems J., van Huffelen A.C. (2003): Measurement of the conductivity of skull, temporarily removed during epilepsy surgery. Brain Topography 16(1):29-38.

Huang M-X, Song T., Hagler D.J., Podgorny I., Jousmaki V., Cui L., Gaa K., Harrington D.L., Dale A.M., Lee R.R., Elman J., Halgren E. (2007): A novel integrated MEG and EEG analysis method for dipolar sources. Neuroimage 37:731-748.

Kaipio J, Somersalo E. (2007): Statistical inverse problems: Discretization, model reduction and inverse crimes. J. Computational and Applied Mathematics 198:493-504.

Khosla D, Don M., Kwong B. (1999): Spatial mislocalization of EEG electrodes - effects on accuracy of dipole estimation. Clin. Neurophysiol. 110:261-271.

Kobayashi K, Yoshinaga H., Oka M., Ohtsuka Y., Gotman J. (2003): A simulation study of the error in dipole source localization for EEG spikes with a realistic head model. Clin. Neurophysiol. 114:1069-1078.

Lai Y, van Drongelen W., Ding L., Hecox K.E., Towle V.L., Frim D.M., He B. (2005): Estimation of in vivo human brain-to-skull conductivity ratio from simultaneous extra- and intra-cranial electrical potential recordings. Clinical Neurophysiology 116:456-465.

Lanfer B, Scherg M., Dannhauer M., Knosche T.R., Burger M., Wolters C.H. (2012): Influences of skull segmentation inaccuracies on EEG source analysis. NeuroImage 62:418-431.

Lew S, Wolters C.H., Anwander A., Makeig S., MacLeod R.S. (2009): Improved EEG source analysis using low-resolution conductivity estimation in a four-compartment finite element head model. Human Brain Mapping 30:2862-2878.

Lucka F, Pursiainen S., Burger M., Wolters C.H. (2012): hierarchical Bayesian inference for the EEG inverse problem using realistic FE head models: Depth localization and source separation for focal primary currents. NeuroImage 61:1364-1382.

Lutkenhoner B, Menninghaus E., Steinstroter O., Wienbruch C., Gilbler H.M., Elbert T. (1995): Neuromagnetic Source Analysis Using Magnetic Resonance Images for the Construction of Source and Volume Conductor Model. Brain Topography 7(4):291-299.

Makeig S, Debener S., Onton J., Delorme A. (2004): Mining event-related brain dynamics. Trends in Cognitive Sciences 8(5):204–210.

Marin G, Guerin C., Baillet S., Garnero L., Meunier G. (1998): Influence of skull anisotropy for the forward and inverse problem in EEG: Simulation studies using FEM on realistic head models. Human Brain Mapping 6(4):250-269.

Meijs J, Weier O., Peters M. J., Van Oosterom A. (1989): On the numerical accuracy of the boundary element method. IEEE Trans. Biomed. Eng. 36:1038-49.

Michel C.M., Murray M.M., Lantz G.L., Gonzalez S., Spinelli L., de Peralta R. G. (2004): EEG source imaging. Clinical Neurophysiology 115:2195-2222.

Mosher J.C., Spencer M.E., Leahy R.M., Lewis P.S. (1993): Error bounds for EEG and MEG dipole source localization. Electroencep. and Clin. Neurophysiol. 86:303-321.

Oostendorp TF, Delbeke J., Stegeman D. F. (2000): The conductivity of the human skull: Results of in vivo and in vitro measurements. IEEE Trans. Biomed. Eng. 47:1487-1492.

Plummer C, Harvey M.C., Cook M. (2008): EEG source localization in focal epilepsy: where are we now? Epilepsia 49(2):201–219.

Ramon C, Schimpf P., Haueisen J. (2006): Influence of head models on EEG simulations and inverse source localizations. Biomedical Eng. Online 6.

Roth BJ, Balish M., Gorbach A., Sato S. (1993): How well does a three-sphere model predict positions of dipoles in a realistically shaped head? Electroenceph. Clin. Neurophysiol. 87:175-184.

Rush S, Driscoll D.A. (1968): Current distribution in the brain from the surface electrodes. Anesthesia and Analgesia, Current res. 47:717-723.

Russell GS, Eriksen K.J., Poolman P., Luu P., Tucker D.M. (2005): Geodesic photogrammetry for localizing sensor positions in dense-array EEG. Clin. Neurophysiol. 116(5):1130-1140.

Sadleir R.J., Argibay A. (2007): Modeling Skull Electrical Properties. Annals of Biomed. Eng. 35(10):1699-1712.

Schneider M. (1974): Effect of inhomogeneities on surface signals coming from a cerebral current dipole source. IEEE Trans. Biomed. Eng. 21(1):52-54.

Shaw JC, Roth M. (1955): Potential distribution analysis II: A theoretical consideration of its significance in terms of electrical field theory. Electroenceph. clin. neurophysiol. 7:285-292.

Ulker Karbeyaz B, Gencer N.G. (2003): Electrical conductivity imaging via contactless measurements: an experimental study. IEEE Trans. Med. Imag. 22:627-635.

Valdes-Hernandez PA, von Ellenrieder N., Ojeda-Gonzales A., Kochen S., Aleman-Gomez Y., Muravchik C., Valdes-Sosa P. A. (2009): Approximate average head models for EEG source imaging. J. of Neuroscience Methods 185:125-132.

Van Uitert R, Johnson C., Zhukov L. (2004): Influence of head tissue conductivity in forward and inverse magnetoencephalographic simulations using realistic head models. IEEE Trans. on Biomed. Eng. 51:2129-2137.

Vanrumste B, Van Hoey G.,Van de Walle R., D'Hav M., Lemahieu I., Boon P. (2000): Dipole location errors in electroencephalogram source analysis due to volume conductor model errors. Med. and Biol. Eng. and Comput 38(5):528-534.

Vatta F, Meneghini F., Esposito F., Mininel S., Di Salle F. (2010): Realistic and Spherical HeadModeling for EEG Forward Problem Solution: A Comparative Cortex-Based Analysis. Comput. Int. and Neuroscience 2010.

Wang Y, Gotman J. (2001): The influence of electrode location errors on EEG dipole source localization with a realistic head model. Clin. Neurophysiol. 112:1777-1780.

Weinberg H, Brickett P., Coolsma F., Baff M. (1986): Magnetic localization of intracranial dipoles: simulation with a physical model. Electroenceph. Clin. Neurophysiol. 64:159-170.

Wendel K, Narra N. G., Hannula M., Kauppinen P., Malmivuo J. (2008): The Influence of CSF on EEG Sensitivity Distributions of Multilayered Head Models. IEEE Trans. Biomed. Eng. 55(4):1454-1456.

Wolters CH, Anwander A, Tricoche X., Weinstein D., Koch M.A., MacLeod R.S. (2006): Influence of tissue conductivity anisotropy on EEG/MEG field and return current computation in a realistic head model: A simulation and visualization study using high-resolution finite element modeling. NeuroImage 30:813-826

Wolters CH, Kuhn M., Anwander A., Reitzinger S. (2002): A parallel algebraic multigrid solver for finite element method based source localization in the human brain. Comput. Visual Sci. 5:165-177.

Yvert B, Bertrand O., Thevenet M., Echallier J. F., Pernier J. (1997): A systematic evaluation of the spherical model accuracy in EEG dipole localization. Electroenceph. Clin. Neurophysiol. 102:352-459.

Zhang Z, Jewett D. (1993): Insidious errors in dipole localization parameters at a single time-point due to model misspecification of number of shells. Electroenceph. Clin. Neurophysiol. 88:1-11.

Zhang Z, Jewett D., Goodwill G. (1994): Insidious errors in dipole parameters due to shell model misspecification using multiple time points. Brain Topography 6:283-298.